



Recent Progress of Quantum Dot Lasers Monolithically Integrated on Si Platform

Victoria Cao, Jae-Seong Park, Mingchu Tang*, Taojie Zhou, Alwyn Seeds, Siming Chen* and Huiyun Liu

Department of Electronic and Electrical Engineering, University College London, London, United Kingdom

With continuously growing global data traffic, silicon (Si)-based photonic integrated circuits have emerged as a promising solution for high-performance Intra-/Inter-chip optical communication. However, a lack of a Si-based light source remains to be solved due to the inefficient light-emitting property of Si. To tackle the absence of a native light source, integrating III-V lasers, which provide superior optical and electrical properties, has been extensively investigated. Remarkably, the use of quantum dots as an active medium in III-V lasers has attracted considerable interest because of various advantages, such as tolerance to crystalline defects, temperature insensitivity, low threshold current density and reduced reflection sensitivity. This paper reviews the recent progress of III-V quantum dot lasers monolithically integrated on the Si platform in terms of the different cavity types and sizes and discusses the future scope and application.

Keywords: Si photonics, quantum dot, molecular beam epitaxy, semiconductor laser, DFB laser, modelocked laser, photonic crystal laser

INTRODUCTION

Si photonics is a key technology to confront the fast-growing data traffic in advanced data-communication network infrastructures, e.g., data centres and high-performance computing [1], replacing current copper interconnectors with optical interconnection on a single chip. {Thomson, 2016 #39}The emerging challenges for transmission, manipulation and storage of voluminous data have motivated extensive research in Si-based photonic components. It enables chip-scale photonic integration with Si microelectronics; however, current state-of-the-art optical transceivers are based on the III-V platform [2, 3]. Indeed, recent developments in Si-based photonic integrated circuits (PICs) have revealed the enhanced device performance and versatile functionality due to its fast transmission rate, broad bandwidth and low power consumption [4]. Moreover, the superior economic advantage of Si from the cheap raw material and complementary metal-oxide-semiconductor (CMOS) compatibility boosts the manufacturing scalability and commercial viability of photonic building blocks, such as waveguide [5, 6], modulators [7, 8], detectors [9, 10], and resonators [11]. However, it remains challenging for group-IV bulk materials to become an efficient light source such as laser diodes and light-emitting diodes due to their indirect bandgap. While significant progress has been made to alleviate the bottleneck for realising Si-based light sources, e.g., porous Si [12], Si nanocrystals [13], Erbium (Er)-doped Si materials [14], Ge-on-Si lasers [15–17], GeSn lasers [18–21] and Si Raman lasers [22–24], failure to operate under electrical pumping conditions or poor device performance, evidenced by the ultra-high threshold current, hinders the practical deployment of group IV-based light emitters. On the other hand, III-V compound semiconductors, due to their excellent optoelectronic properties, render them promising

OPEN ACCESS

Edited by:

Bei Shi,
University of California, Santa Barbara,
United States

Reviewed by:

Bowen Song,
University of California, Santa Barbara,
United States
Yichen Shuai,
National Institute of Standards and
Technology (NIST), United States

*Correspondence:

Mingchu Tang
mingchu.tang.11@ucl.ac.uk
Siming Chen
siming.chen@ucl.ac.uk

Specialty section:

This article was submitted to
Optics and Photonics,
a section of the journal
Frontiers in Physics

Received: 20 December 2021

Accepted: 24 January 2022

Published: 14 February 2022

Citation:

Cao V, Park J-S, Tang M, Zhou T,
Seeds A, Chen S and Liu H (2022)
Recent Progress of Quantum Dot
Lasers Monolithically Integrated on
Si Platform.
Front. Phys. 10:839953.
doi: 10.3389/fphy.2022.839953

candidates for reliable laser sources on Si for future all-optical integration and optoelectronic integrated circuits. With the aid of recent advances in well-established and well-functioning III-V lasers—particularly, quantum-dot (QD) lasers—on Si, the development of Si-based PICs will revolutionise not only the optical communication system but also other application fields such as sensing [25], imaging [26], metrology [27], quantum computing [28] and automotive light detection and ranging [29].

Hybrid and monolithic integration are commonly discussed to realise high-performance III-V lasers integrated on Si substrate. Even though the hybrid integration has been well established by using wafer bonding techniques and has already been commercialised by Intel and other leading industry companies, monolithic integration is regarded as a feasible low-cost, larger-scale, and higher yield integration solution. However, the main challenge of the monolithic integration is the material dissimilarities between III-V materials and group-IV materials; for instance, a high density of threading dislocations (TDs) is generated due to the large lattice mismatch. Recently, the combination of defect-tolerant QD as an active region and strained layers as a defect filter layer has been extensively studied for demonstrating high-performance and reliable Si-based on-chip light sources.

In this paper, we will start by reviewing the challenges and solutions in the monolithic integration and discuss the importance of QDs as an active region in **Section 2**. Then, in **Section 3**, the recent demonstration of QD edge-emitting lasers grown on Si substrate is reviewed and discussed in terms of different cavity configurations, e.g., Fabry-Perot (FP), distributed feedback (DFB) and mode-locked lasers. The recent remarkable results of micro and nanoscale Si-based QD lasers with different microcavities are presented in **Section 4**. The final section gives a brief discussion and conclusion to the whole review paper.

MONOLITHIC INTEGRATION OF III-V QD LASERS ON SI

Over the past decades, significant efforts have been devoted to integrating III-V active materials on Si, the method of which can be generally classified into two categories: heterogeneous integration and monolithic integration [29]. Although the heterogeneous approach has been intensively studied and sufficiently matured to be commercially adopted by industry, this approach still has limitations, including expensive, small-sized III-V substrates and low integration density [30]. In this regard, the monolithic integration, capable of providing economically efficient mass production and dense integration, has attracted substantial interest recently [31]. Moreover, the defect-tolerable III-V QD lasers have demonstrated the feasibility of direct growth of III-V on Si. Indeed, recent experiments show evidence that the performance and reliability of QD lasers grown on Si are now approaching those on native III-V substrate, which underpins the commercial feasibility of this method [32]. Therefore, the monolithically integrated III-V QD lasers on Si are the most promising light source, fulfilling the

cost-competitive and large-scale production demand for the booming Si photonics market.

Challenges of Monolithic Integration

The well-known practical problem of monolithic integration is the generation of crystalline defects from significant material dissimilarities between III-V materials and Si substrate. These defects act as non-radiative recombination centres and shunt paths in the fabricated device, which significantly degrades the device performance [33]. In addition, the lifetime and maximum operation temperature are also constricted because the defects grow under ageing conditions, attributed to the recombination-enhanced climb process [34]. The main issues of heteroepitaxial growth of III-V on Si are stated as follows: 1) Antiphase boundaries (APBs) and antiphase domains (APDs) are generated due to the growth of polar III-V on non-polar Si and monatomic steps on the surface of Si substrate, as shown in the atomic force microscopy (AFM) image of **Figure 1A**. 2) A high density of TDs is generated along with misfit dislocations because of large lattice mismatch. **Figure 1B** shows that while the most of misfit dislocations are concentrated on the III-V/Si interface, the TDs propagate into the III-V material. 3) During the cooling down process, thermal cracks are formed to relax the accumulated thermal stress caused by the difference in thermal expansion coefficient, as shown in **Figure 1C**.

Various methods have been conducted to reduce defect density to assure high-performance, long-term reliability devices. One representative approach to diminish APBs is the use of miscut Si substrates with a slight 4°–6° offcut angle from the (001) orientation. This is because the structural reconstruction of monatomic steps to double-atomic, which is believed to be responsible for suppressing the formation of APBs, can be achieved by high-temperature annealing and surface treatment [35]. With the offcut Si substrates, for example, QD lasers achieved impressive continuous-wave (CW) lasing results, including the lowest reported threshold current density of 62.5 A/cm² (4° offcut silicon substrate) [36] and the highest recorded maximum operation temperature of 119°C (the 6° offcut substrate with Ge buffer layer) [37]. However, these results are achieved at the expense of their CMOS compatibility, which is one of the significant benefits of Si photonics. For standard CMOS processing, the miscut angle of silicon substrates should be less than 0.5°. To date, implementing intermediate buffer layers (e.g., Ge, GaP and GaAs) [38–40] and patterned Si substrate [41, 42] has been widely developed to obtain APB-free III-V on on-axis Si substrates. Still, the involvement of the metal-organic chemical vapor deposition (MOCVD) in both processes, particularly for the growth of QD lasers, complicates the device manufacturing procedure and increases the cost because most of QD laser structures are typically grown by molecular beam epitaxy (MBE) system which has been proved as an ideal method to grow the QD. In other words, the APB-free MOCVD-grown buffers on on-axis Si still require the use of MBE system in order to obtain high-quality QD lasers. Meanwhile, direct growth using only MBE process without intermediate buffer layers or patterned Si has also been progressed to suppress the formation of APBs by carefully

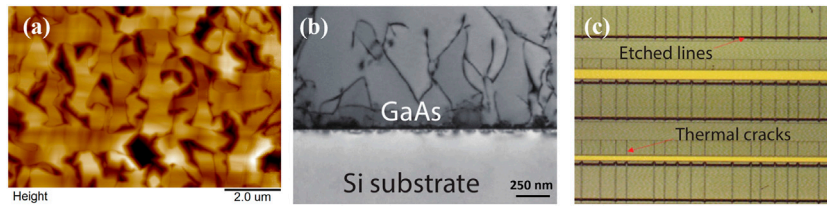


FIGURE 1 | (A) AFM image of APBs. **(B)** Bright-field scanning TEM image of TDs. **(C)** Top-view microscopy image of thermal cracks on the wafer surface. Reproduced with permission from Ref. [33].

TABLE 1 | comparison between MBE and MOCVD epitaxial growth.

	Background doping	Growth Temperature	Regrowth difficulty	Selective area growth	Precise growth control	Multi-wafer growth
MBE	Low	Middle	High	Difficult	High	Low
MOCVD	High	High	Low	Easy	Medium	High

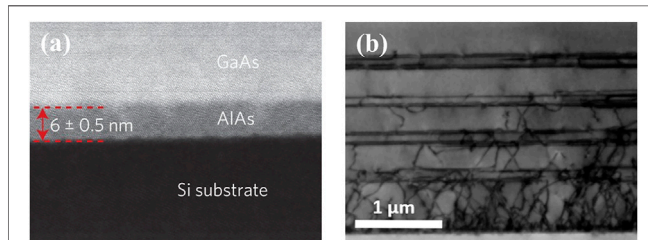


FIGURE 2 | (A) Dark-field scanning TEM image of the 6 nm AlAs nucleation layer. **(B)** Bright-field scanning TEM image of the buffer layer, including DFLs. Reproduced with permission from [36].

optimising the growth condition and buffer layer [43–45]. Recently, MOCVD and MBE are both widely used in scientific research and industrial production, and they have proved successful in the heteroepitaxial growth of III-V materials on the Si platform. However, the use of MOCVD and MBE focuses on the different areas due to their unique properties. A detailed comparison of MBE and MOCVD is presented in **Table 1**.

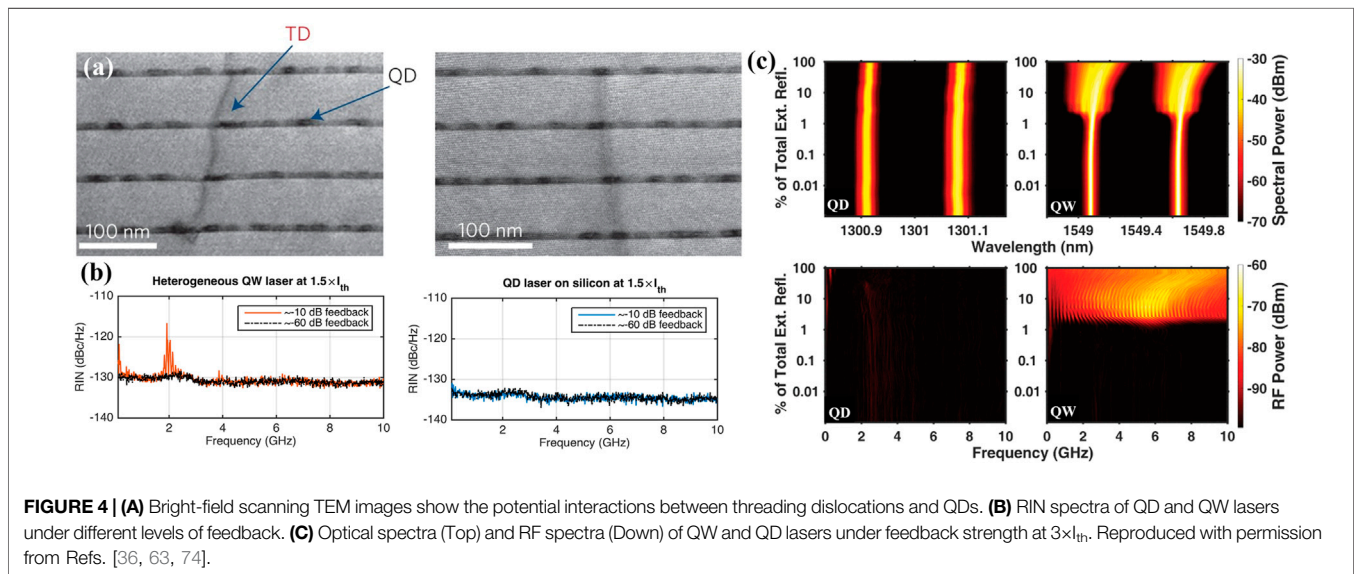
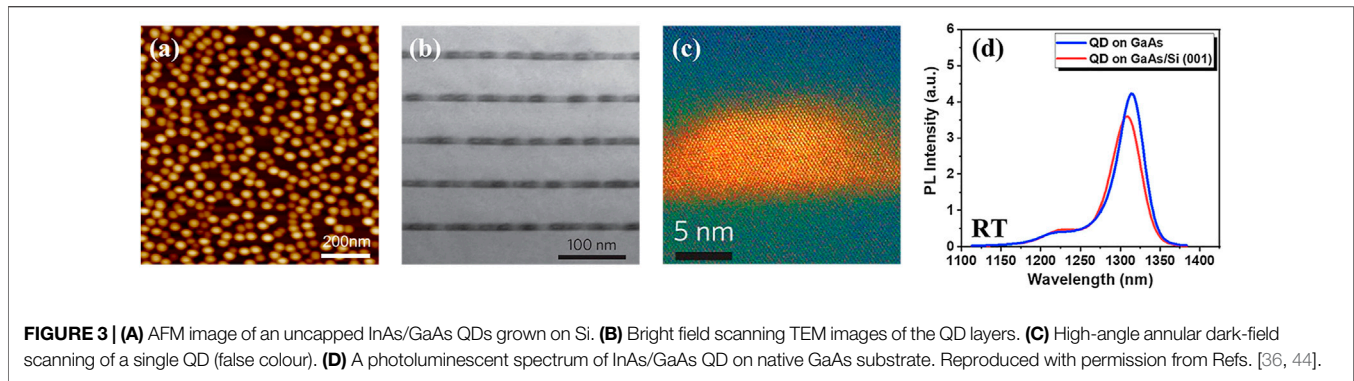
To reduce threading dislocation density (TDD), thermal cycle annealing and strained-layer superlattices (SLSs) as dislocation filter layers (DFLs) are commonly adopted [46]. The SLSs restrict the upward propagation of TDs by bending them laterally and thus promoting self-annihilation, while thermal cycle annealing supplies enough kinetic energy to accelerate this process. The growth of an III-V nucleation layer on Si substrate also reduces TDD and the surface's flattening [47]. **Figures 2A,B** show cross-sectional transmission electron microscopy (TEM) images of an AlAs nucleation layer and DFLs, respectively. **Figure 2A** shows that a thin AlAs layer offers a very smooth interface for subsequent growth of the GaAs layer (36). As shown in **Figure 2B**, the propagation of TDs is effectively inhibited by increasing the number of DFLs. All MBE-grown III-Vs on the 4° offcut Si [36], and the on-axis Si with AlGaAs nucleation layers

[43] produce the TDDs of $\sim 10^5 \text{ cm}^{-2}$ and $4.7 \times 10^7 \text{ cm}^{-2}$, respectively. The use of v-groove patterned Si substrate [48] and GaP intermediate layer [49], along with the utilisation of SLSs and thermal cycle annealing, also exhibits low TDDs of $3 \times 10^6 \text{ cm}^{-2}$ and $7 \times 10^6 \text{ cm}^{-2}$, respectively. However, since the TDD of III-V on native GaAs substrate gives a value of $10^3\text{--}10^4 \text{ cm}^{-2}$ [31], which is a few orders of magnitude lower than that on Si substrate, there is still space for reducing the TDD to enhance the laser performance further.

The presence of thermal micro-cracks in the epilayer should also be considered because this leads to restriction in the growth thickness of III-V material. Solutions to release this thermal stress experienced during growth temperature variation include the engineering of strain profile [50], selective area growth and growth on the deeply patterned Si substrates [51, 52].

Advantages of QDs

With the advent of modern QD engineering technology, III-V lasers have an exciting opportunity to further improve their performances through the unique quantum confinement effect of QD. The nanostructured semiconductor QDs are confined in all three dimensions on the order of the de Broglie wavelength, typically 7–70 nm [53]. Due to the restriction of carrier momentum, all available energy states in QD exist at discrete states, which results in a delta function-like density of state (DoS). Hence, this effective carrier localisation reduces transparency current density and lower threshold current than quantum-well (QW) lasers [54]. In addition, the thermal energy distribution of electrons in the quantised DoS is significantly decreased, which makes the QD temperature-insensitive compared with other higher dimensional structures [31]. This is experimentally proved by the maximum operating temperatures of QD lasers on GaAs native and Si substrates as high as 220°C [55] and 130°C [56], respectively, which are well beyond the requirement in datacom and telecom applications; for instance, a typical operating condition in data centres is $\sim 80^\circ\text{C}$.



Finally, it is worth mentioning that the emission wavelength of InAs QDs is suitable for Si photonics, which avoids the band-edge absorption of Si waveguides.

After the idea of QD was first theoretically proposed in 1982 [57], it was not until 1994 that experimental verification of semiconductor QDs was reported *via* the Stranski-Krastanov (S-K) growth method [58]. The S-K growth begins with a layer-by-layer growth and then switches to the island growth above a certain critical thickness to relax the strain. The shape of QDs is often either lens-shaped or truncated pyramid-shaped. **Figures 3A–C** present the scanning images of InAs/GaAs dot-in-well structure obtained through AFM, bright field and high-angle annular dark-field TEM techniques, respectively. The AFM indicates a dot density around $4.0 \times 10^{10} \text{ cm}^{-2}$, while each layer of the dot is separated by a $\sim 50 \text{ nm}$ of GaAs material. A typical QD is around 10 nm height and 20 nm width. The size and shape of the QD influence the degree of confinement of charge carriers. As the size of QD increases, the transition energy level—the bandgap—decreases. Therefore, small-sized QDs emit light at a shorter wavelength with higher energies; on the contrary, large dots emit light at a longer wavelength [59].

Therefore, an ensemble of QDs grown in a self-organised manner results in an inhomogeneously broadened gain spectrum due to the fluctuation of the dot dimension. **Figure 3D** shows the photoluminescence (PL) spectrum of InAs/GaAs QDs on native GaAs and Si substrates. The spectral width of inhomogeneous broadening can be determined from the PL spectrum. The peak PL intensity of QD on GaAs/Si is lower than that on native GaAs substrate, with a slight blue-shift, mainly because of the increased number of crystalline defects. There is a broad range of tunability for QD properties, such as dot density, size, shape and homogeneity. With stringent control of material composition and growth conditions, the property of QDs can be tailored to the specific need for a wide range of applications.

The high tolerance to defect in QD devices is of paramount importance for the direct growth of III-V on Si because many defects are inevitably generated during the heteroepitaxial growth. For instance, unlike the QW structure, the propagation of TDs towards the surface can affect only a restricted number of QDs, leaving most of QDs intact and continuously workable [36]. **Figure 4A** shows the possible

interactions between TDs and QDs through scanning TEM measurement. In addition, the strain field around QDs can bend the upward propagation of TDs underneath the QDs [60, 61]. Moreover, typical carrier diffusion lengths for QD and QW systems at room temperature (RT) are $\sim 1\ \mu\text{m}$ and several microns, respectively. Owing to the reduced carrier diffusion length, the carriers in QDs are unlikely to interact with defects, thus minimising the surface recombination effect. In general, under ageing conditions, defects experience recombination-enhanced climb effect that degrades the lifetime and reliability of the device. This phenomenon was observed by the extension of misfit dislocation, generation of dislocation loops and point defects proximate to the misfit dislocations [34]. However, it was found that the dislocation climb effect was slower in a QD system [62]. This climb inhibition is mainly due to the effective carrier localisation within self-assembled QDs, which reduces the number of carriers escaping from the dots and thus limits the occurrence of non-radiative recombination events such as Shockley-Read-Hall (SRH) recombination and Auger recombination [62].

The employment of QDs also provides better dynamic properties, such as low relative intensity noise (RIN) and linewidth enhancement factor (LEF), compared with the QW structure [63, 64]. In the optical communication system, a low RIN is desired to improve the data transmission rate and distance with a high signal-to-noise ratio (SNR) and low bit-error-rate (BER). To date, the RIN values as low as $-160\ \text{dB/Hz}$ in both GaAs-based and InP-based QD lasers have been reported [65, 66]. For the Si-based QD lasers, the RIN values between $-150\ \text{dB/Hz}$ and $-160\ \text{dB/Hz}$ have been published [67]. **Figure 4B** compares RIN spectra measured in the 0–10 GHz range between QW and QD lasers [63]. The QD laser demonstrates a stable RIN spectrum over a wide range of frequencies, whereas large spikes are identified in the QW laser. In addition to the RIN, the LEF is also an important parameter that affects the laser performance, including narrow spectral linewidth, enhanced feedback insensitivity and low-frequency chirp during high-speed modulation. The QD can theoretically have a predicted zero LEF due to the perfectly symmetrical gain curve according to the Kramers-Kronig relationship [68]. However, in practical QD lasers, several factors, such as inhomogeneous distribution of QDs and crystal defects, cause a non-zero LEF value [69, 70]. Nonetheless, a near-zero LEF of 0.13 can be attained in QD lasers [71], which is much lower than the typical values of 2–5 in QW lasers [72, 73]. Interestingly, the QD structure can obtain a negative LEF value. In this case, zero LEF can be achieved by increasing the bias level because LEF increases with current injection above threshold due to gain clamping [68].

External optical feedback (EOF) has detrimental effects on the device performance, such as linewidth broadening, coherence collapse, increased phase noise, and mode hopping at high current [63]. The QDs are proved to have a strong tolerance to the optical feedback due to low LEF and high damping factor [75]. **Figure 4C** shows the optical and RF spectra of QD and QW lasers biased at $3 \times I_{\text{th}}$ under various feedback strengths [74]. The QW experienced a more considerable broadening in the optical mode than the QD. In the RF mode, intense nonlinear oscillations

were observed in the QW laser, implying that the laser enters the coherence collapse regime, whereas nothing was identified in the QD laser. All these observations confirm higher feedback immunity of QD than QW. The capability of high tolerance to optical feedback paves the way for establishing isolator-free integration, reducing the packaging complexity, device footprint and energy consumption.

P-type Modulation Doping in QDs

Despite the superior theoretical performance of QD lasers, a weak confinement of the holes leads to a degradation in performance at high operating temperatures [68]. To provide more holes to the QD active region, a P-type modulation doping technique was proposed and developed by researchers from the University of Texas, Austin [76–78]. Indeed, the employment of p-modulation doping in the active region is now well known for improving the thermal performance of QD lasers. This is usually done by adding Be into a GaAs spacer layer to provide extra holes. The spacer layer separates each QD layer for strain relaxation and avoids electronic coupling between layers. The thermal broadening of charge carriers controls the temperature sensitivity. In III-V materials, the hole confinement in the QD is much smaller in respect to the electron confinement due to heavier effective mass and tightly spaced energy levels in the valence band (VB) [71]. Consequently, holes can easily be thermalised and escape from the dot. By adding extra holes into the active region, the quasi-Fermi level in VB is lowered, which eases the condition for population inversion [79]. As a result, the gain and temperature stability are improved, but at the cost of increased threshold and decreased slope efficiency at RT due to increased optical loss by higher carrier absorption and increased non-radiative recombination [68]. However, as temperature increases to a certain critical value, the threshold of p-doped QD laser becomes lower than that of the unintentionally doped lasers. It is worth mentioning that the LEF of the p-doped QD laser is smaller than the undoped. As the concentration of p-doping increases from 0 to $1 \times 10^{18}\ \text{cm}^{-3}$, LEF decreases from 0.48 to a negative value of -0.66 [29]. A recent study also found that for p-doped QD lasers, the RIN level is very stable across temperatures ranging from 15 to 35°C with a minimum value of $-150\ \text{dB/Hz}$ [80]. The concentration of p-doping needs to be optimised, as the performance improvement slows down with increased concentration of p-dopant due to increased rate of non-radiative recombination and scattering process, accompanied by the state-filling effect [81].

EDGE-EMITTING QD LASERS ON SILICON

Edge-emitting lasers emit light horizontally along the axis of the cavity. In this configuration, the light travels in a more extended gain medium, thus providing higher output power than surface-emitting lasers. **Figure 5** illustrates the recent progress in the threshold current for various edge-emitting InAs/GaAs QD lasers monolithically grown on Si, including basic FP lasers, mode-locked lasers (MLLs), DFB lasers and tunable lasers. All values are

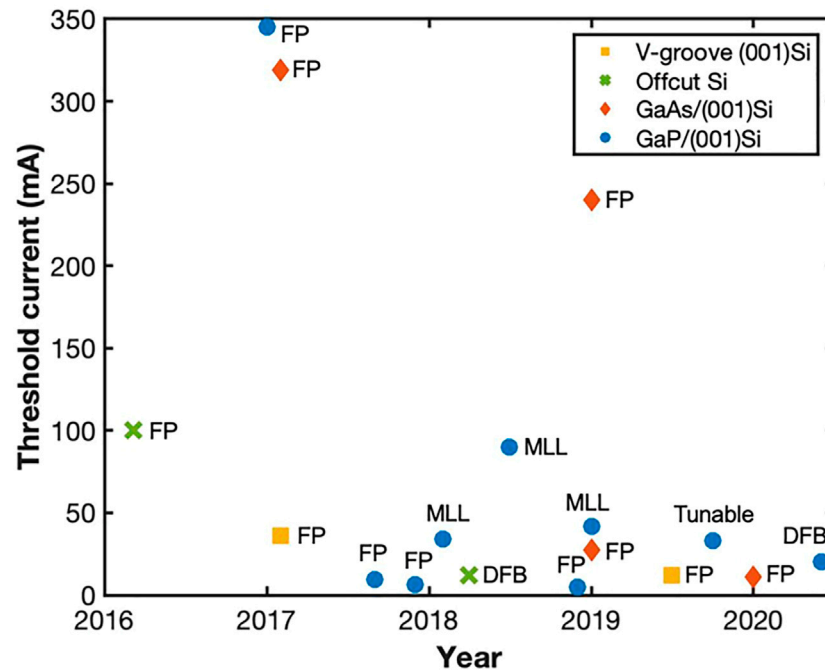


FIGURE 5 | Recent developments of threshold current for QD lasers monolithically grown on silicon.

taken under CW operation at RT. Not surprisingly, the threshold current shows a decreasing trend no matter which method is used to suppress the formation of APDs. This can be attributed to gradually enhanced QD growth, including QD density and uniformity, along with the development of high-quality buffer layers to reduce TDD in the epilayer. The more advanced device structure and fabrication technique may further enhance the performance, e.g., high-reflection coating on the as-cleaved facet to reduce mirror loss, high-quality metallisation to reduce series resistance, and better heat dissipation technology to surpass the gain limitation at high current.

FP Laser

Since the first demonstration of 1.3 μm InAs/GaAs QD lasers on 4° offcut Si substrate under pulsed operation by Wang et al. from UCL in 2011 [47], a CW operation of QD lasers on offcut Si was realised with a drastic reduction in threshold current density to 62.5 A/cm² and increased output power of >100 mW from a single facet, *via* the improved buffer layer design and epitaxial growth technique in 2016 [36]. Subsequently, the first CW electrically pumped InAs/GaAs QD lasers on on-axis (001) Si was reported in 2017 [45]. However, they suffered from a relatively high threshold current density of 425 A/cm² and a low maximum operating temperature of 36°C. Recently, these lasing parameters were significantly improved to 160 A/cm² and 52°C, respectively, by the same group, optimising the buffer design and growth condition [44].

Besides intensively studied broad area lasers, narrow ridge lasers that guarantee fundamental transverse electronic mode lasing are now garnering more attention [82–84]. Reducing the

ridge width down to a few microns, a lower threshold current and better heat dissipation are also expected due to the reduced injection area and efficient current confinement. However, the sidewall recombination effect becomes significant along with the increase in series resistance. For instance, Kwon et al. [43] reported CW InAs/GaAs QD lasers directly grown on on-axis Si, which operate at over 100°C without implementing p-doped active region from the University of Tokyo [43]. In this work, neither intermediate buffer layer nor patterned substrate was applied, and the device dimension was 1,100 × 7 μm , producing a reasonable threshold current density of 370 A/cm². UCSB reported further improvement on reducing TDD to 3 × 10⁷ cm⁻², and narrow ridge width lasers achieved a threshold current (density) as low as 11 mA (173 A/cm²) and maximum operating temperature of up to 80°C [85].

Table 2 summarises the recent achievements of III-V FP lasers on Si, including the material quality as quantised by TDD and device structure. The operating wavelength range is focused on O-band due to the utilisation of InAs/GaAs QDs. Although C-band operation based on the InP platform is also crucial for mid/long-haul communication, the progress of 1.55 μm QD lasers on Si has been hindered by far more significant lattice mismatch between InP and Si than that between GaAs and Si [86, 87]. Indeed, unlike QD lasers grown on InP native substrate, C-band QD lasers on on-axis (001) Si can operate only under pulsed injection with a high threshold current density of 1.6 kA/cm² due to high TDD and rough epilayer surface [88]. Furthermore, the typical TDD of InP on Si is on the order of 10⁸ cm⁻² [88]. Therefore, 1.55 μm CW electrically pumped QD lasers on Si remain to be further explored.

TABLE 2 | recent progress of III-V FP QD lasers epitaxially grown on silicon.

Year	Substrate	TDD (cm ⁻²)	Device structure (μm ²)	Operation condition	(μm)	J _{th} (A/cm ²)	T _{max} (°C)	References
2014	6° offcut Ge/Si	10 ⁸ (P-TEM)	FP ((700–1,200)×(4–12), HR coated)	RT (pulsed/cw)	1.25	362/430	130/119	[37]
2016	4° offcut Si	10 ⁸ (P-TEM)	FP (3,200 × 50, as cleaved)	RT (cw)	1.32	62.5	75	[36]
2017	GaP/Si (001)	3 × 10 ⁸ (ECCI)	FP (2000 × 20, as cleaved)	RT (cw)	1.28	862	90	[89]
2017	v-grooved Si (001)	7 × 10 ⁷ (ECCI)	FP (1,200 × 6, HR coated 95%/0)	RT (cw)	1.25	500	80	[90]
2017	GaP/Si (001)	7.3 × 10 ⁶ (ECCI)	FP (2,600 × 8, HR coated 95%/0)	RT (cw)	1.27	132	80	[91]
2017	Si (001)	NA	FP (3,000 × 25, as cleaved)	RT (pulsed/cw)	1.29	240/425	102/36	[45]
2018	Si (001)	3 × 10 ⁷ (X-TEM)	FP (2000 × 80, as cleaved)	RT(pulsed)	1.25	320	70	[92]
2018	GaP/Si (001)	7 × 10 ⁶	FP (1,174 × 2.5, HR coated 99%/60%)	RT (cw)	1.3	164	85	[93]
2019	Si (001)	NA	FP (3,000 × 50, as cleaved)	RT(cw)	1.33	160	52	[44]
2019	Si (001)	4.7 × 10 ⁷ (P-TEM)	FP (1,100 × 7, as cleaved)	RT(cw)	1.22	370	101	[43]
2019	v-grooved Si (001)	3 × 10 ⁶ (ECCI)	FP (1,450 × 10, HR coated 99%/0)	RT(cw)	1.28	286	80	[48]
2020	Si (001)	3 × 10 ⁷ (ECCI)	FP (1,270 × 6, as cleaved)	RT(cw)	1.27	173	80	[85]
2020	Ge/Si	4 × 10 ⁶ (ECCI)	FP (3,000 × 25, as cleaved)	RT(pulsed)	1.28	200	130	[56]

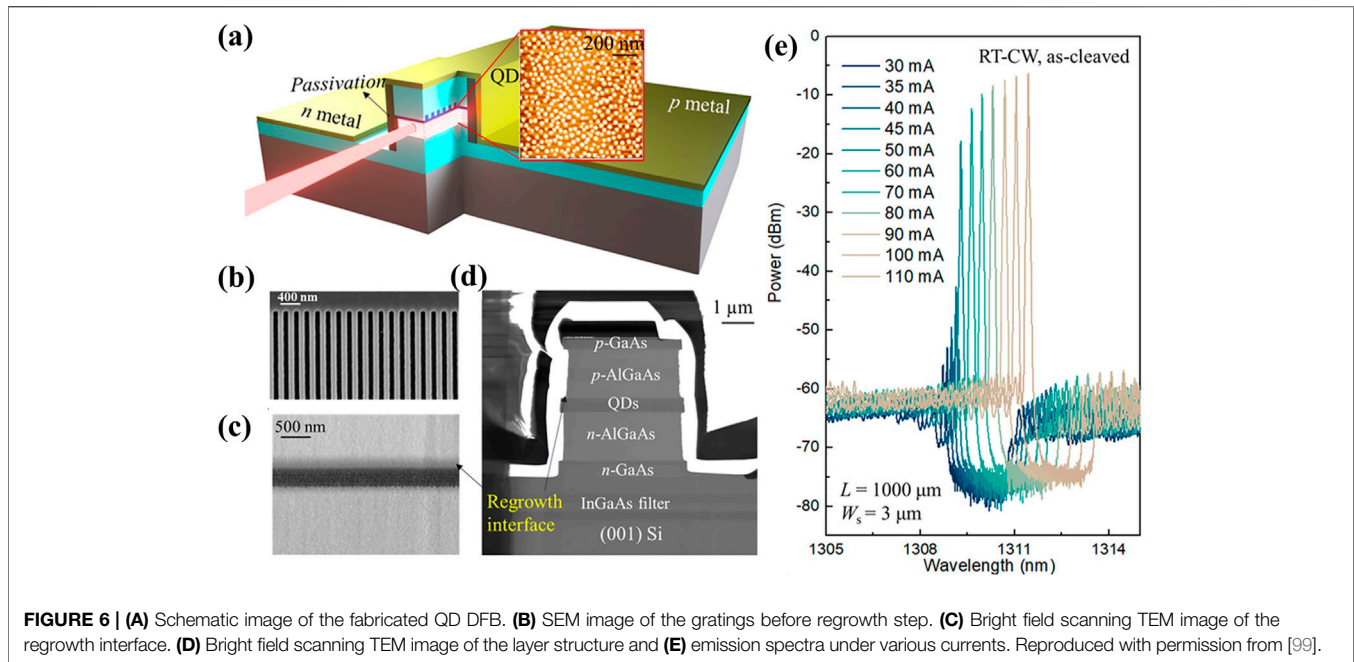


FIGURE 6 | (A) Schematic image of the fabricated QD DFB. **(B)** SEM image of the gratings before regrowth step. **(C)** Bright field scanning TEM image of the regrowth interface. **(D)** Bright field scanning TEM image of the layer structure and **(E)** emission spectra under various currents. Reproduced with permission from [99].

Note. HR, RT, CW, J_{th} and T_{max} stand for high reflection, room temperature, continuous-wave, threshold current density, and maximum operating temperature.

A. DFB Lasers

DFB lasers, an array of single-longitudinal-mode lasers, cover a wide range of wavelengths with a high side-mode suppression ratio (SMSR) and high mode stability [94]. The individual wavelength channels and channel spacing of DFB lasers can be controlled by changing the gratings. Therefore, they have been widely employed as a light source for wavelength division multiplexing (WDM) systems [95, 96].

The first InP DFB laser monolithically grown on Si was demonstrated by Wang et al. at Ghent university in 2015. The Si-based O-band QD DFB array was also shown by employing the selective area growth technique achieved by the same research group in the following year [97]. However, these devices are limited by optical pumping and small wavelength coverage. In 2018, UCL and SUN Yat-sen University researchers demonstrated the first electrically pumped InAs/GaAs QD DFB laser array monolithically integrated on Si [98]. In this work, an array of six devices exhibits a high SMSR of 50 dB, O-band wavelength coverage of 100 nm, and channel spacing of 20 nm, satisfying the requirement of a commercial WDM system. However, the use of 4° offcut Si substrate inhibits the compatibility with CMOS foundries.

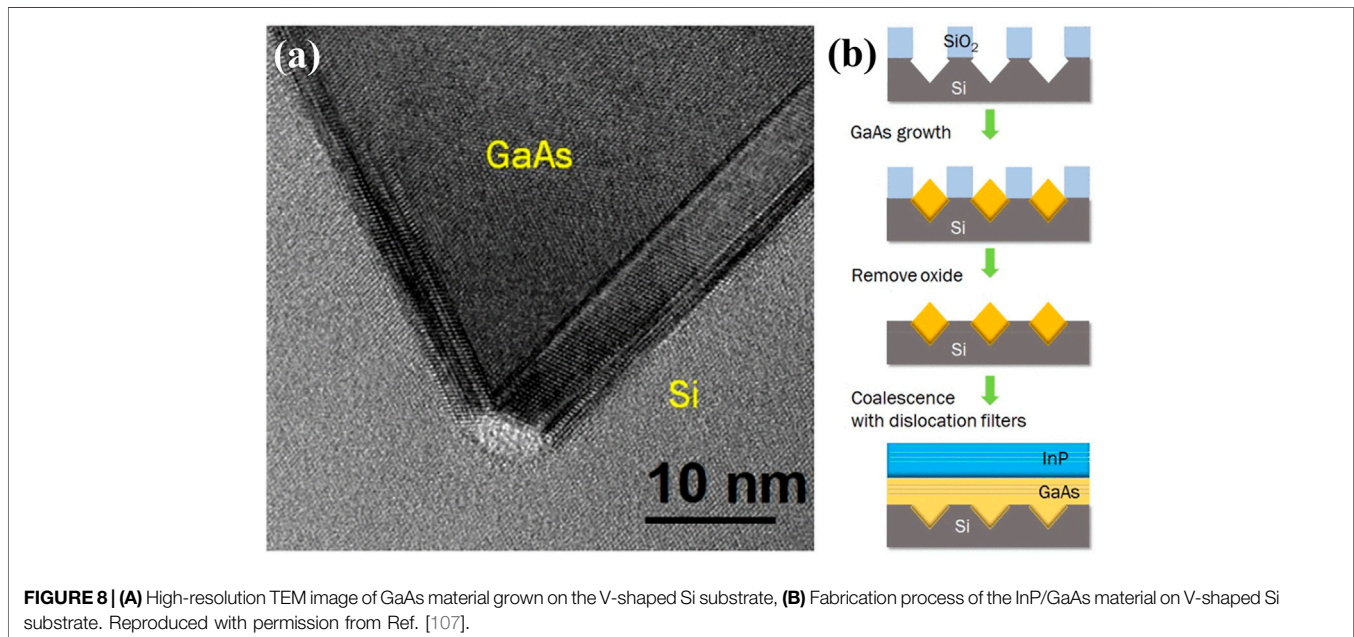
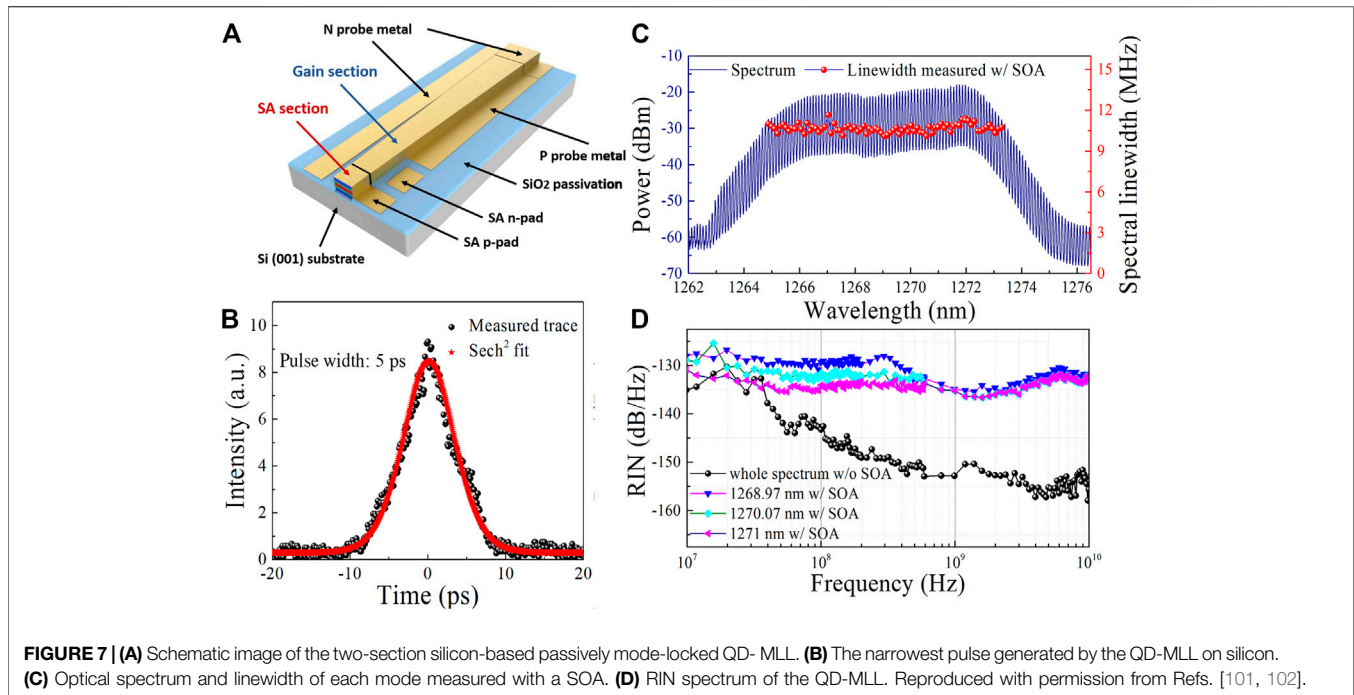
The first O-band QD DFB lasers monolithically grown on on-axis (001) Si substrate were demonstrated in 2020 [99]. **Figure 6A** presents a schematic illustration of QD lasers. In this work, the GaP/Si template was used to suppress the formation of APDs, and a low TDD of $7.3 \times 10^6 \text{ cm}^2$ was achieved. As a result, a high QD density of over 5×10^{10} was observed in the inset of **Figure 6A**. **Figures 6B–D** illustrate scanning electron microscope (SEM)

images of the grating before regrowth and bright-field TEM images of regrowth interface and whole laser structure, respectively. In **Figure 6E**, emission spectra at various current injections were presented. The fabricated lasers demonstrated CW lasing operation with a threshold current of 20 mA (threshold current density of 440 A/cm^2) at RT, a maximum output power of 4.4 mW, and a maximum operating temperature of 70°C. In particular, the maximum output is much larger than the previously reported DFB laser (0.5 mW) [98]. In addition, the wavelength coverage over 50 nm (1,285–1,338 nm) and SMSR of more than 50 dB were achieved from a five-wavelength QD DFB laser array.

B. Mode-locked Lasers

In addition to the DFB lasers, a single MLL, which allows multiple-wavelength emission simultaneously with stable channel spacing, has also been regarded as another appealing on-chip WDM light source. The MLLs simplify the packaging process and reduce the cost and system loss [100]. Furthermore, the unique properties of QDs, including inhomogeneous broadening, ultrafast gain recovery, and low amplified spontaneous emission (ASE) noise, are of great importance for high-performance MLLs. Accordingly, much effort has been focused on fabricating QD MLLs with a high repetition rate, short pulse duration, and low timing jitter over the ultrawide gain spectrum.

A QD MLL on Si with a repetition rate of 20 GHz was demonstrated in 2019 [101]. The GaP/Si template and chirped QD system were employed in this work. Unlike single-wavelength lasers with narrow linewidth, the MLL requires a broad gain spectrum that can cover a wide range of wavelengths. Therefore, to extend the gain bandwidth, the thickness of the capping layer and emission wavelength of each QD layer was carefully



controlled, resulting in a PL full width at half maximum (FWHM) of 69 nm. **Figure 7A** shows that the conventional two-section deeply etched device with a ridge width of 3 μm and device length of 2048 μm was fabricated. The saturable absorber (SA) section was 14% of the total device length, and no coating was applied on both facets. The threshold current at RT was measured to be 42 mA under CW operation. The fabricated device produced ultra-short pulses with a 20 GHz repetition rate, minimum pulse duration of 5 ps (**Figure 7B**), RF linewidth of 1.8 kHz and a low timing jitter value of 82.7 fs.

In **Figure 7C**, the optical spectrum measured with a semiconductor optical amplifier (SOA) showed a 3 dB bandwidth of 6.1 nm with 51 channels and 10 dB bandwidth with 80 channels. As shown in **Figure 7D**, the average RIN of the entire spectrum was -152 dB/Hz, measured from 10 MHz to 10 GHz. Terabit transmission experiment was also performed with 32 Gb and PAM-4 signals. Using 64-wavelength channels transmit with relatively low BERs, an aggregate total transmission capacity of 4.1 Tbit/s was measured.

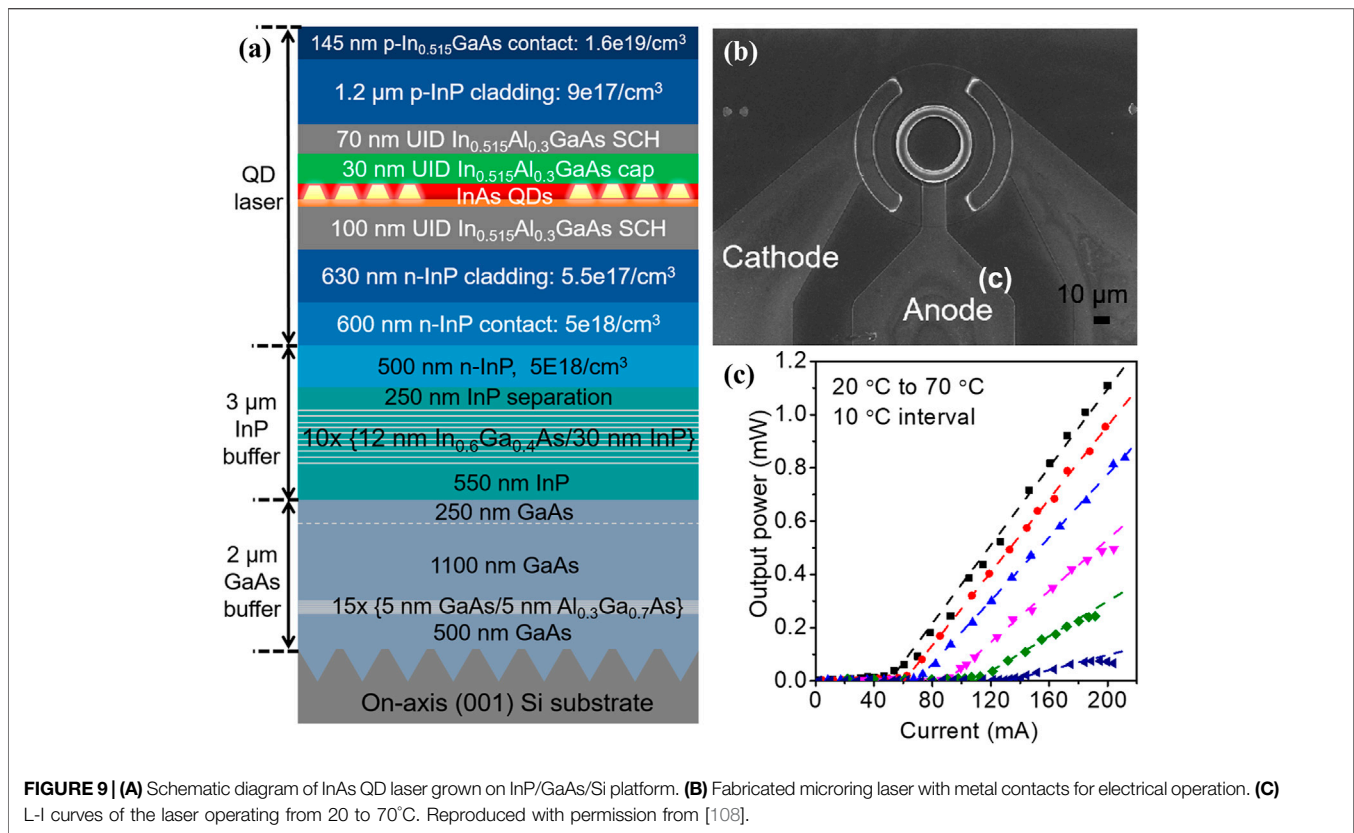


FIGURE 9 | (A) Schematic diagram of InAs QD laser grown on InP/GaAs/Si platform. **(B)** Fabricated microring laser with metal contacts for electrical operation. **(C)** L-I curves of the laser operating from 20 to 70°C. Reproduced with permission from [108].

QD LASERS WITH MICROCAVITY ON SILICON

Using Si micro and nanoscale photonics technology as an inter-chip optical connector is vital to realise quantum computing, optoelectronic integrated circuits, and an optical microprocessor [1, 103]. However, developing an inter-chip optical connector requires a Si-based, small-footprint, high-quality, and low energy consumption light source. Although the Si-based ridge-waveguide lasers with QD active region have been extensively investigated in recent years, their large size is incompatible with the micro and nanoscale photonic integrated circuits (nanoPICs). On the other hand, semiconductor lasers with a microcavity, such as a microring and a microdisk, have superior optical properties of ultra-low threshold and high-quality factor (Q-factor) due to the low-loss high-quality whispery gallery modes (WGM). Moreover, monolithically integrated III-V lasers with a microscale footprint can further increase the integration density of a single laser device on a Si chip. Furthermore, the unique property of ultra-low operating power of such microlaser can further reduce the energy cost for a new type of inter-chip optical connection, which supplies laser source for nanoPIC. However, integrating such microdisk and microring lasers directly on the Si platform *via* the monolithic method requires a proper growth strategy, as we mentioned in the previous sessions.

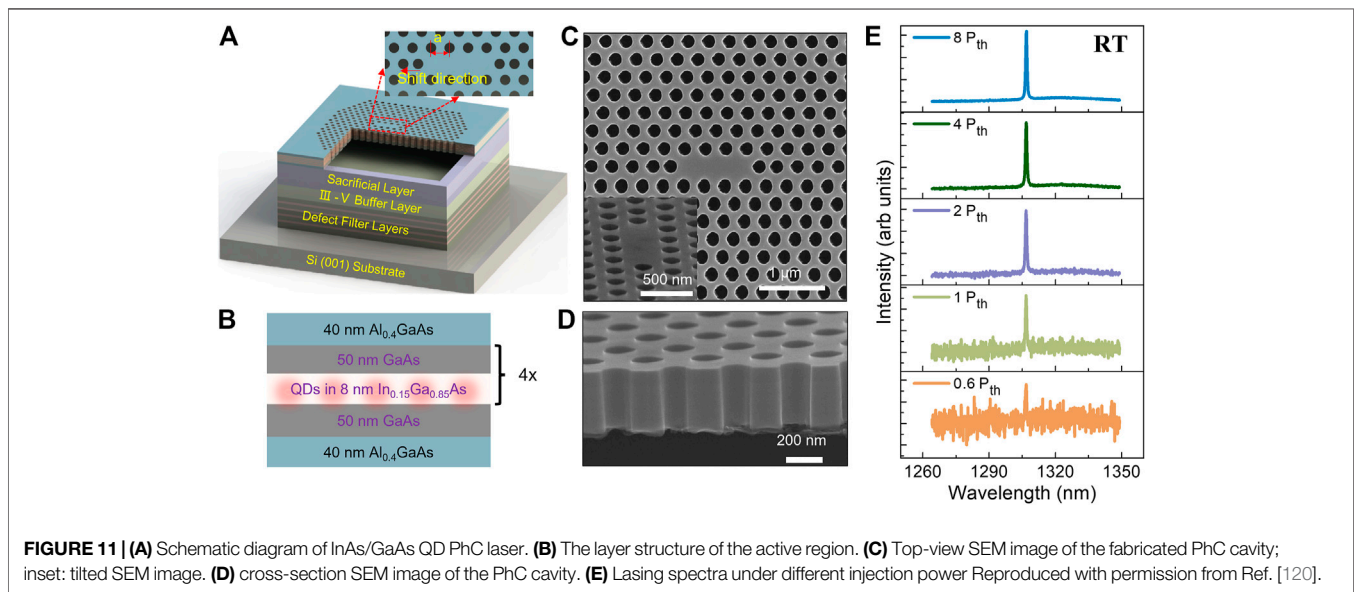
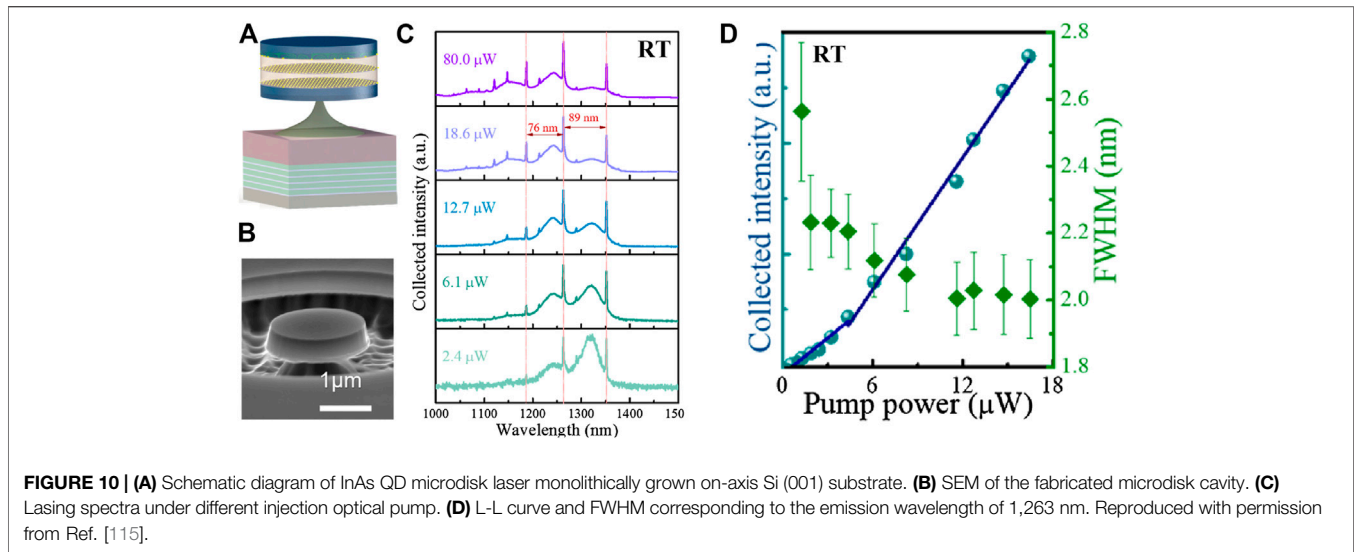
Another type of nano-laser, using photonic crystal (PhC) as a cavity, has recently attracted substantial interest because of its

advantages, such as strong spontaneous emission rate, single-mode operation, and ultra-low energy consumption. In addition, the PhC laser is also considered a potential candidate for a nanoscale light source of nanoPICs and integration with other small microelectronic components on a single Si chip. In this section, recent works on the Si-based QD laser with different types of microcavity are reviewed and discussed.

Microring Laser

Recently, Si-based microring lasers using InAs QDs as an active region have been well exploited. Researchers from Hong Kong University of Science and Technology and the University of California, Santa Barbara, demonstrated MOCVD-grown strain-relaxed and high-quality GaAs and InP buffer layers on the V-shaped on-axis (001) Si substrate [104–106]. To obtain this platform, the V-groove shape is first lithographically defined *via* line openings on a (001) Si substrate using SiO₂ growth mask, while the SiO₂ stripes lie along the [110] direction. Then, the V-shaped trenches with <111> facets were formed by using KOH etching [106]. As seen in **Figure 8A** a high density of defects is generated at the interface of the GaAs and Si within a region of 10 nm thickness [107], while the twisted defects are trapped at the tip of the Si ridge. As a result, visibly defect-free GaAs is obtained inside the V-shape. Finally, as shown in **Figure 7B**, the thin-film structure is grown by removing the SiO₂ layer and then growing the flat GaAs and InP layers.

Based on this platform, 1.3 and 1.55 μm electrically pumped InAs QD microring lasers were developed with high operating



temperature and low threshold [108–112]. C-band microring laser will be focused on in this review paper, as the O-band microring lasers have been reviewed extensively [32, 113]. In 2019, Si et al., who demonstrated electrically pumped 1.5 μm InP-based QD microring lasers grown on InP/GaAs/Si platform, reported a TDD at a low level of 10^8 cm^{-2} after growing three sets of the InGaAs/InP strained-layer as a defect filter layer on the platform [108]. As presented in **Figure 9A**, a QD laser structure was grown on the optimised InP/GaAs/Si platform, which consists of five layers of InAs/InAlGaAs QD active region embedded between 630 nm-thick InP n-type cladding layer and 1.2 μm InP-thick p-type cladding layer. The microring cavity was formed by using inductively coupled plasma reactive ion etching (ICP-RIE) deep etching technique, followed by N- and P-type metal

deposition of Ti/Pt/Au and Ge/Au/Ni/Au, respectively. An 800 nm thick SiO_2 passivation layer was then deposited on the microring structure by plasma-enhanced chemical vapour deposition system. The fabricated microring laser with a cavity radius of 25 μm is presented in the SEM image of **Figure 9B**.

The laser device was tested under pulsed mode with different operating temperatures (up to 70°C), as shown in **Figure 9C**. The threshold current and slope efficiency reached 50 mA and 0.0075 W/A at RT, respectively. The characteristic temperature, T_0 , was measured to be 51.5 K. Although the state-of-the-art microlaser device for Si photonics requires CW operation and operating temperature over 75°C, this result is still a remarkable progress, which can be further enhanced by reducing the TDD and improving the quality of sidewall.

Microdisk Laser

QD laser with microdisk cavity, which is another ideal candidate for an on-chip light source in Si photonics, has recently been extensively developed due to its less on-chip space, low-power-consumption on dynamic and static, compared with microring laser [114]. In 2019, Zhou et al. demonstrated 1.3 μm microdisk lasers directly grown on on-axis Si (001) substrate with a few micrometre diameters [115]. To achieve high-performance III-V lasers monolithically integrated on Si substrate, a 400 nm APD-free GaAs layer was grown on the on-axis Si substrate by using MOCVD. The Si double-atomic steps were created by using hydrogen annealing at 1,200°C, which suppresses the formation of APD [116]. After the growth of the GaAs buffer layer, the wafer was sent to the MBE system for the subsequent step growth. Then, the four sets of InGaAs/GaAs SLS DFLs are grown to further reduce the TDD to the level of 10^6 cm^{-2} [117, 118], followed by a 1 μm $\text{Al}_{0.6}\text{Ga}_{0.4}\text{As}$ sacrificial layer. The active region consists of three layers of InAs/GaAs QD grown on a 2 nm InGaAs QW and capped by a 4 nm of InGaAs layer. Each layer of the QDs was separated by 50 nm-thick, high temperature grown GaAs material [119].

The microdisk cavity was fabricated by the ICP-RIE technique. **Figure 10A** presents a schematic illustration of the fabricated microdisk cavity. The fabricated cavity only has a diameter of around 2 μm , as shown in **Figure 10B**. The lasing spectra are presented in **Figure 10C**, indicating that three lasing peaks are observed at 1,187 nm, 1,263 nm and 1,352 nm. The L-L curve in **Figure 10D** shows the threshold optical power of $\sim 2.6 \pm 0.4 \mu\text{W}$ and the reduced FWHM with the injection optical pump power increase.

Photonic Crystal Laser

Compared with microdisk and microring cavities, the PhC cavity has better control of the light confinement due to the high Q-factor, ultrasmall mode volume (V_{mode}) and large Purcell factor (proportional to Q/V_{mode}), as well as ultralow energy consumption due to the enhanced light-matter interaction. Those superior properties encourage the PhC laser to implement Si-based nanoPICs as an on-chip high-efficiency light source.

Recently, Zhou et al. demonstrated QD lasers grown on Si platform with 2D photonic crystal cavity, as schematically shown in **Figure 11A** [120]. Four layers of the dot-in-well structure were grown on a GaAs/Si on-axis (001) substrate, embedded within two sets of 40 nm $\text{Al}_{0.4}\text{Ga}_{0.6}\text{As}$ and 50 nm GaAs guiding layers, as shown in **Figure 11B**. The PhC pattern was defined by electron beam lithography and fabricated by using ICP-RIE dry etching to obtain the air-hole through the top to the sacrificial layer, as shown in **Figure 10C** and inset. The lattice constant of the fabricated PhC is 310 nm with an air-hole radius of 0.27, as the total size of the PhC is a few micrometres. In **Figure 11D**, it is found that some residuals are left on the sidewall of PhC due to the wet etching process. The PhC laser was measured under CW optical pumping by a 632.8 nm He-Ne laser. **Figure 11E** presents lasing spectra under different excitation power from 0.6 to 8 times threshold power, indicating a single-mode emission with FWHM of 0.68 nm at a threshold power of 0.6 μW . The demonstrated

results prove the feasibility of using a PhC laser as a nanoscale light source for the inter-chip optical interconnects.

DISCUSSION AND CONCLUSION

This paper reviews the recent progress of monolithically integrated III-V QD lasers on Si platforms. Owing to the superior properties of QD and the optimised growth strategy, high-performance FP, DFB and mode-locked edge-emitting lasers grown on the Si platform have been demonstrated, while the performances are comparable to the devices grown on III-V native substrates in terms of the ageing, threshold, power, SMSR, etc. It can be concluded that the Si-based edge-emitting lasers are good enough to be off-chip light sources for Si photonics. However, it is still challenging for those lasers to be deployed as an on-chip light source due to the relatively thick buffer layer, which increases the difficulty of coupling the light into Si waveguides and other optical components on Si-on-insulator platform. The following research goal of this area will be to develop an efficient light coupling method between the lasers and waveguides; for example, reducing the buffer thickness can maximise the feasibility of light coupling, using selective area growth technique to create an in-plane coupling between the lasers and waveguides. To further reduce the cost of using modulator in the PICs, a higher direct modulation speed of QD lasers needs to be developed, as the current QW lasers already demonstrate over 50 GHz direct modulation speed [121, 122].

The Si-based micro and nanoscale lasers have also been developed recently due to their potential applications, including an optical microprocessor, quantum computing, optoelectronic integrated circuits, etc. Despite the successful demonstration of the electrically pumped operation of the microring and microdisk lasers on Si *via* monolithic and hybrid integration methods [123, 124], an electrically pumped PhC laser directly grown on Si substrate has not been demonstrated yet, compared with the hybrid integration method [125, 126]. To realise a practical QD-based micro/nano laser on Si, electrically pumped operation along with fast modulation speed, high SMSR, and long lifetime needs to be established. Furthermore, a proper integration strategy needs to develop to combine the micro/nanoscale laser with microelectronic devices integrated by back-end technology [127].

AUTHOR CONTRIBUTIONS

VC, J-SP, and MT proposed and wrote this manuscript. TZ, AS, SC, and HL review and modified the manuscript.

FUNDING

UK Engineering and Physical Sciences Research Council (EP/T01394X/1 and EP/P006973/1); National Epitaxy Facility; Royal Academy of Engineering (RF201617/16/28); European Project H2020- ICT-PICTURE (780930). SC acknowledges the Royal Academy of Engineering for funding his Research Fellowship.

REFERENCES

- Thomson D, Zilkie A, Bowers JE, Komljenovic T, Reed GT, Vivien L, et al. Roadmap on Silicon Photonics. *J Opt* (2016) 18:073003. doi:10.1088/2040-8978/18/7/073003
- Nagarajan R, Kato M, Pleumeekers J, Evans P, Corzine S, Hurtt S, et al. InP Photonic Integrated Circuits. *IEEE J Select Top Quan Electron*. (2010) 16(5): 1113–25. doi:10.1109/jstqe.2009.2037828
- Liang D, Bowers JE. Photonic Integration: Si or InP Substrates. *Electron Lett* (2009) 45(12):578–81. doi:10.1049/el.2009.1279
- Asghari M, Krishnamoorthy AV. Energy-efficient Communication. *Nat Photon* (2011) 5(5):268–70. doi:10.1038/nphoton.2011.68
- Heck MJR, Bauters JF, Davenport ML, Spencer DT, Bowers JE. Ultra-low Loss Waveguide Platform and its Integration with Silicon Photonics. *Laser Photon Rev* (2014) 8(5):667–86. doi:10.1002/lpor.201300183
- Bauters JF, Davenport ML, Heck MJR, Doyle JK, Chen A, Fang AW, et al. Silicon on Ultra-low-loss Waveguide Photonic Integration Platform. *Opt Express* (2013) 21(1):544–55. doi:10.1364/oe.21.000544
- Reed GT, Mashanovich G, Gardes FY, Thomson DJ. Silicon Optical Modulators. *Nat Photon* (2010) 4(8):518–26. doi:10.1038/nphoton.2010.179
- Timurdogan E, Sorace-Agaskar CM, Sun J, Shah Hosseini E, Biberman A, Watts MR. An Ultralow Power Athermal Silicon Modulator. *Nat Commun* (2014) 5(1):4008–11. doi:10.1038/ncomms5008
- Mauthe S, Baumgartner Y, Sousa M, Ding Q, Rossell MD, Schenk A, et al. High-speed III-V Nanowire Photodetector Monolithically Integrated on Si. *Nat Commun* (2020) 11(1):4565–7. doi:10.1038/s41467-020-18374-z
- Park H, Fang AW, Jones R, Cohen O, Raday O, Sysak MN, et al. A Hybrid AlGaInAs-Silicon Evanescent Waveguide Photodetector. *Opt Express* (2007) 15(10):6044–52. doi:10.1364/oe.15.006044
- Baehr-Jones T, Hochberg M, Walker C, Scherer A. High-Q Optical Resonators in Silicon-On-Insulator-Based Slot Waveguides. *Appl Phys Lett* (2005) 86:081101. doi:10.1063/1.1871360
- Koshida N, Koyama H. Visible Electroluminescence from Porous Silicon. *Appl Phys Lett* (1992) 60(3):347–9. doi:10.1063/1.106652
- Cazzanelli M, Navarro-Urriós D, Riboli F, Daldosso N, Pavesi L, Heitmann J, et al. Optical Gain in Monodispersed Silicon Nanocrystals. *J Appl Phys* (2004) 96(6):3164–71. doi:10.1063/1.1781770
- Yerci S, Li R, Dal Negro L. Electroluminescence from Er-Doped Si-Rich Silicon Nitride Light Emitting Diodes. *Appl Phys Lett* (2010) 97:081109.
- Liu J, Kimerling LC, Michel J. Monolithic Ge-On-Si Lasers for Large-Scale Electronic-Photonic Integration. *Semiconductor Sci Technol* (2012) 27: 094006.
- Liu J, Sun X, Camacho-Aguilera R, Kimerling LC, Michel J. Ge-on-Si Laser Operating at Room Temperature. *Opt Lett* (2010) 35(5):679–81. doi:10.1364/OL.35.000679
- Liu J, Sun X, Pan D, Wang X, Kimerling LC, Koch TL, et al. Tensile-strained, N-type Ge as a Gain Medium for Monolithic Laser Integration on Si. *Opt Express* (2007) 15(18):11272–7. doi:10.1364/OE.15.011272
- Zhou Y, Miao Y, Ojo S, Tran H, Abernathy G, Grant JM, et al. Electrically Injected GeSn Lasers on Si Operating up to 100 K. *Optica* (2020) 7(8):924–8. doi:10.1364/OPTICA.395687
- Margetis J, Zhou Y, Dou W, Grant PC, Alharthi B, Du W, et al. All Group-IV SiGeSn/GeSn/SiGeSn QW Laser on Si Operating up to 90 K. *Appl Phys Lett* (2018) 113(22):221104. doi:10.1063/1.5052563
- Al-Kabi S, Ghetmiri SA, Margetis J, Pham T, Zhou Y, Dou W, et al. An Optically Pumped 2.5 μm GeSn Laser on Si Operating at 110 K. *Appl Phys Lett* (2016) 109(17):171105. doi:10.1063/1.4966141
- Wirths S, Geiger R, von den Driesch N, Mussler G, Stoica T, Mantl S, et al. Lasing in Direct-Bandgap GeSn alloy Grown on Si. *Nat Photon* (2015) 9(2): 88–92. doi:10.1038/nphoton.2014.321
- Rong H, Xu S, Kuo Y-H, Sih V, Cohen O, Raday O, et al. Low-threshold Continuous-Wave Raman Silicon Laser. *Nat Photon* (2007) 1(4):232–7. doi:10.1038/nphoton.2007.29
- Rong H, Jones R, Liu A, Cohen O, Hak D, Fang A, et al. A Continuous-Wave Raman Silicon Laser. *Nature* (2005) 433(7027):725–8. doi:10.1038/nature03346
- Rong H, Liu A, Jones R, Cohen O, Hak D, Nicolaescu R, et al. An All-Silicon Raman Laser. *Nature* (2005) 433(7023):292–4. doi:10.1038/nature03273
- Subramanian AZ, Ryckeboer E, Dhakal A, Peyskens F, Malik A, Kuyken B, et al. Silicon and Silicon Nitride Photonic Circuits for Spectroscopic Sensing On-A-Chip [Invited]. *Photon Res* (2015) 3(5):B47–B59. doi:10.1364/prj.3.000b47
- Rogers C, Piggott AY, Thomson DJ, Wiser RF, Opris IE, Fortune SA, et al. A Universal 3D Imaging Sensor on a Silicon Photonics Platform. *Nature* (2021) 590(7845):256–61. doi:10.1038/s41586-021-03259-y
- Coddington I, Swann WC, Nenadovic L, Newbury NR. Rapid and Precise Absolute Distance Measurements at Long Range. *Nat Photon* (2009) 3(6): 351–6. doi:10.1038/nphoton.2009.94
- JW Silverstone, J Wang, D Bonneau, P Sibson, R Santagati, C Erven, et al. editors. *Silicon Quantum Photonics*. IEEE (2016). 2016 International Conference on Optical MEMS and Nanophotonics (OMN).
- Norman JC, Jung D, Zhang Z, Wan Y, Liu S, Shang C, et al. A Review of High-Performance Quantum Dot Lasers on Silicon. *IEEE J Quan Electron*. (2019) 55(2):1–11. doi:10.1109/jqe.2019.2901508
- Liu AY, Bowers J. Photonic Integration with Epitaxial III-V on Silicon. *IEEE J Select Top Quan Electron*. (2018) 24(6):1–12. doi:10.1109/jstqe.2018.2854542
- Liao M, Chen S, Park J-S, Seeds A, Liu H. III-V Quantum-Dot Lasers Monolithically Grown on Silicon. *Semicond Sci Technol* (2018) 33(12): 123002. doi:10.1088/1361-6641/aae6a5
- H Deng, K Li, M Tang, J Wu, M Liao, Y Lu, et al. editors. *III-V Quantum Dot Lasers Monolithically Grown on Silicon*. 2019 Optical Fiber Communications Conference And Exhibition (OFC), 2019 (2019). p. 3–7.
- Pan S, Cao V, Liao M, Lu Y, Liu Z, Tang M, et al. Recent Progress in Epitaxial Growth of III-V Quantum-Dot Lasers on Silicon Substrate. *J Semicond* (2019) 40(10):101302. doi:10.1088/1674-4926/40/10/101302
- Jung D, Norman J, Wan Y, Liu S, Herrick R, Selvidge J, et al. Recent Advances in InAs Quantum Dot Lasers Grown on on-Axis (001) Silicon by Molecular Beam Epitaxy. *Phys Status Solidi A* (2019) 216(1):1800602. doi:10.1002/pssa.201800602
- Kroemer H. Polar-on-nonpolar Epitaxy. *J Cryst Growth* (1987) 81(1): 193–204. doi:10.1016/0022-0248(87)90391-5
- Chen S, Li W, Wu J, Jiang Q, Tang M, Shutt S, et al. Electrically Pumped Continuous-Wave III-V Quantum Dot Lasers on Silicon. *Nat Photon* (2016) 10(5):307–11. doi:10.1038/nphoton.2016.21
- Liu AY, Zhang C, Norman J, Snyder A, Lubyshev D, Fastenau JM, et al. High Performance Continuous Wave 1.3 μm Quantum Dot Lasers on Silicon. *Appl Phys Lett* (2014) 104:041104.
- Volz K, Beyer A, Witte W, Ohlmann J, Németh I, Kunert B, et al. GaP-nucleation on Exact Si (001) Substrates for III/V Device Integration. *J Cryst Growth* (2011) 315(1):37–47. doi:10.1016/j.jcrysgro.2010.10.036
- Kunert B, Németh I, Reinhard S, Volz K, Stolz W. Si (001) Surface Preparation for the Antiphase Domain Free Heteroepitaxial Growth of GaP on Si Substrate. *Thin Solid Films* (2008) 517(1):140–3. doi:10.1016/j.tsf.2008.08.077
- Németh I, Kunert B, Stolz W, Volz K. Heteroepitaxy of GaP on Si: Correlation of Morphology, Anti-phase-domain Structure and MOVPE Growth Conditions. *J Cryst Growth* (2008) 310(7–9):1595–601. doi:10.1016/j.jcrysgro.2007.11.127
- Wang Z, Tian B, Pantouvaki M, Guo W, Absil P, Van Campenhout J, et al. Room-temperature InP Distributed Feedback Laser Array Directly Grown on Silicon. *Nat Photon* (2015) 9(12):837–42. doi:10.1038/nphoton.2015.199
- Wan Y, Li Q, Geng Y, Shi B, Lau KM. InAs/GaAs Quantum Dots on GaAs-On-V-Grooved-Si Substrate with High Optical Quality in the 1.3 μm Band. *Appl Phys Lett* (2015) 107:081106. doi:10.1063/1.4929441
- Kwoen J, Jang B, Watanabe K, Arakawa Y. High-temperature Continuous-Wave Operation of Directly Grown InAs/GaAs Quantum Dot Lasers on on-axis Si (001). *Opt Express* (2019) 27(3):2681–8. doi:10.1364/oe.27.002681
- Li K, Liu Z, Tang M, Liao M, Kim D, Deng H, et al. O-band InAs/GaAs Quantum Dot Laser Monolithically Integrated on Exact (0 0 1) Si Substrate. *J Cryst Growth* (2019) 511:56–60. doi:10.1016/j.jcrysgro.2019.01.016
- Chen S, Liao M, Tang M, Wu J, Martin M, Baron T, et al. Electrically Pumped Continuous-Wave 13 Mm InAs/GaAs Quantum Dot Lasers Monolithically

- Grown on on-axis Si (001) Substrates. *Opt Express* (2017) 25(5):4632–9. doi:10.1364/OE.25.004632
46. Tournié E, Cerutti L, Rodriguez J-B, Liu H, Wu J, Chen S. Metamorphic III-V Semiconductor Lasers Grown on Silicon. *MRS Bull* (2016) 41(3):218–23. doi:10.1557/mrs.2016.24
 47. Wang T, Liu H, Lee A, Pozzi F, Seeds A. 13- μm InAs/GaAs Quantum-Dot Lasers Monolithically Grown on Si Substrates. *Opt Express* (2011) 19(12):11381–6. doi:10.1364/OE.19.011381
 48. Shang C, Gossard AC, Bowers JE, Wan Y, Norman JC, Collins N, et al. Low-Threshold Epitaxially Grown 1.3- μm InAs Quantum Dot Lasers on Patterned (001) Si. *IEEE J Select Top Quan Electron*. (2019) 25(6):1–7. doi:10.1109/jstqe.2019.2927581
 49. Jung D, Zhang Z, Norman J, Herrick R, Kennedy M, Patel P, et al. Highly Reliable Low-Threshold InAs Quantum Dot Lasers on on-axis (001) Si with 87% Injection Efficiency. *ACS Photon* (2017) 5(3):1094–100.
 50. Wang B, Bao S, Made RI, Lee KH, Wang C, Lee KEK, et al. Control Wafer bow of InGaP on 200 Mm Si by Strain Engineering. *Semicond Sci Technol* (2017) 32(12):125013. doi:10.1088/1361-6641/aa952e
 51. Huang H, Ren X, Lv J, Wang Q, Song H, Cai S, et al. Crack-free GaAs Epitaxy on Si by Using Midpatterned Growth: Application to Si-Based Wavelength-Selective Photodetector. *J Appl Phys* (2008) 104(11):113114. doi:10.1063/1.3035843
 52. Scaccabarozzi A, Binetti S, Acciarri M, Isella G, Campesato R, Gori G, et al. Integration of InGaP/GaAs/Ge Triple-junction Solar Cells on Deeply Patterned Silicon Substrates. *Prog Photovolt: Res Appl* (2016) 24(10):1368–77. doi:10.1002/ppa.2798
 53. Mitin VV, Kochelap VA, Kochelap VA, Strosio MA. *Introduction to Nanoelectronics: Science, Nanotechnology, Engineering, and Applications*. Cambridge, United Kingdom: Cambridge University Press. (2008).
 54. Liu AY, Srinivasan S, Norman J, Gossard AC, Bowers JE. Quantum Dot Lasers for Silicon Photonics [Invited]. *Photon Res* (2015) 3(5):B1–B9. doi:10.1364/prj.3.0000b1
 55. Nishi K, Takemasa K, Sugawara M, Arakawa Y. Development of Quantum Dot Lasers for Data-Com and Silicon Photonics Applications. *IEEE J Select Top Quan Electron*. (2017) 23(6):1–7. doi:10.1109/jstqe.2017.2699787
 56. Yang J, Liu Z, Jurczak P, Tang M, Li K, Pan S, et al. All-MBE Grown InAs/GaAs Quantum Dot Lasers with Thin Ge Buffer Layer on Si Substrates. *J Phys D: Appl Phys* (2020) 54:035103. doi:10.1088/1361-6463/abb49
 57. Arakawa Y, Sakaki H. Multidimensional Quantum Well Laser and Temperature Dependence of its Threshold Current. *Appl Phys Lett* (1982) 40(11):939–41. doi:10.1063/1.92959
 58. Kirstaedter N, Grundmann M, Richter U, Ustinov VM, Kop'ev PS, Bimberg D, et al. Low Threshold, Large to Injection Laser Emission from (InGa)As Quantum Dots. *Elect Lett* (1994) 30(17):1416–7. doi:10.1049/el:19940939
 59. Chen S. *Hybrid Quantum Well/Quantum Dot Structure for Broad Spectral Bandwidth Emitters*. Sheffield, United Kingdom: University of Sheffield (2014).
 60. Mi Z, Yang J, Bhattacharya P, Qin G, Ma Z. High-performance Quantum Dot Lasers and Integrated Optoelectronics on Si. *Proc IEEE* (2009) 97(7):1239–49. doi:10.1109/jproc.2009.2014780
 61. Ovid'Ko IA. Relaxation Mechanisms in Strained Nanoislands. *Phys Rev Lett* (2002) 88:046103. doi:10.1103/PhysRevLett.88.046103
 62. Mukherjee K, Selvidge J, Jung D, Norman J, Taylor AA, Salmon M, et al. Recombination-enhanced Dislocation Climb in InAs Quantum Dot Lasers on Silicon. *J Appl Phys* (2020) 128:025703. doi:10.1063/1.5143606
 63. Liu AY, Komljenovic T, Davenport ML, Gossard AC, Bowers JE. Reflection Sensitivity of 13 μm Quantum Dot Lasers Epitaxially Grown on Silicon. *Opt Express* (2017) 25(9):9535–43. doi:10.1364/oe.25.009535
 64. Zhang Z, Jung D, Norman JC, Chow WW, Bowers JE. Linewidth Enhancement Factor in InAs/GaAs Quantum Dot Lasers and its Implication in Isolator-free and Narrow Linewidth Applications. *IEEE J Select Top Quan Electron*. (2019) 25(6):1–9. doi:10.1109/jstqe.2019.2916884
 65. Capua A, Rozenfeld L, Mikhelashvili V, Eisenstein G, Kuntz M, Laemmlin M, et al. Direct Correlation Between a Highly Damped Modulation Response and Ultra Low Relative Intensity Noise in an InAs/GaAs Quantum Dot Laser. *Opt Express* (2007) 15(9):5388–93. doi:10.1364/OE.15.005388
 66. Lu Z, Liu J, Mao L, Poole P, Liu E, Weber J, et al. *Inas/Inp Quantum Dot Coherent Comb Lasers Their Applications Data Centre Coherent Communication Systems: SPIE*. (2021).
 67. Liao M, Chen S, Liu Z, Wang Y, Ponnampalam L, Zhou Z, et al. Low-noise 13 μm InAs/GaAs Quantum Dot Laser Monolithically Grown on Silicon. *Photon Res* (2018) 6(11):1062–6. doi:10.1364/PRJ.6.001062
 68. Norman JC, Zhang Z, Jung D, Shang C, Kennedy M, Dumont M, et al. The Importance of P-Doping for Quantum Dot Laser on Silicon Performance. *IEEE J Quan Electron*. (2019) 55(6):1–11. doi:10.1109/jqe.2019.2941579
 69. Qasaimeh O. Effect of Inhomogeneous Line Broadening on Gain and Differential Gain of Quantum Dot Lasers. *IEEE Trans Electron Devices* (2003) 50(7):1575–81. doi:10.1109/ted.2003.813907
 70. Melnik S, Huyet G, Uskov A. The Linewidth Enhancement Factor α of Quantum Dot Semiconductor Lasers. *Opt Express* (2006) 14(7):2950–5. doi:10.1364/OE.14.002950
 71. Duan J, Huang H, Jung D, Zhang Z, Norman J, Bowers JE, et al. Semiconductor Quantum Dot Lasers Epitaxially Grown on Silicon with Low Linewidth Enhancement Factor. *Appl Phys Lett* (2018) 112(25):251111. doi:10.1063/1.5025879
 72. Osinski M, Buus J. Linewidth Broadening Factor in Semiconductor Lasers--An Overview. *IEEE J Quan Electron*. (1987) 23(1):9–29. doi:10.1109/jqe.1987.1073204
 73. Rideout W, Yu B, LaCourse J, York PK, Beernink KJ, Coleman JJ. Measurement of the Carrier Dependence of Differential Gain, Refractive index, and Linewidth Enhancement Factor in Strained-layer Quantum Well Lasers. *Appl Phys Lett* (1990) 56(8):706–8. doi:10.1063/1.102688
 74. Duan J, Huang H, Dong B, Jung D, Norman JC, Bowers JE, et al. 1.3- μm M Reflection Insensitive InAs/GaAs Quantum Dot Lasers Directly Grown on Silicon. *IEEE Photon Technol Lett* (2019) 31(5):345–8. doi:10.1109/lpt.2019.2895049
 75. JC Norman, S Liu, Y Wan, Z Zhang, C Shang, JG Selvidge, et al. editors. *Epitaxial Integration of High-Performance Quantum-Dot Lasers on silicon* International Society for Optics and Photonics (2020).
 76. Deppe DG, Huang H, Shchekin OB. Modulation Characteristics of Quantum-Dot Lasers: the Influence of P-type Doping and the Electronic Density of States on Obtaining High Speed. *IEEE J Quan Electron*. (2002) 38(12):1587–93. doi:10.1109/jqe.2002.805246
 77. Shchekin OB, Deppe DG. 1.3 μm InAs Quantum Dot Laser with To=161 K from 0 to 80 °C. *Appl Phys Lett* (2002) 80(18):3277–9. doi:10.1063/1.1476708
 78. Shchekin OB, Deppe DG. Low-threshold High-T/sub 0/ 1.3- μm InAs Quantum-Dot Lasers Due to P-type Modulation Doping of the Active Region. *IEEE Photon Technol Lett* (2002) 14(9):1231–3. doi:10.1109/lpt.2002.801597
 79. Zhang Z, Jung D, Norman JC, Patel P, Chow WW, Bowers JE. Effects of Modulation P Doping in InAs Quantum Dot Lasers on Silicon. *Appl Phys Lett* (2018) 113:061105. doi:10.1063/1.5040792
 80. Duan J, Zhou Y, Dong B, Huang H, Norman JC, Jung D, et al. Effect of P-Doping on the Intensity Noise of Epitaxial Quantum Dot Lasers on Silicon. *Opt Lett* (2020) 45(17):4887–90. doi:10.1364/ol.395499
 81. Zhang Z, Jung D, Norman JC, Patel P, Chow WW, Bowers JE. Effects of Modulation P Doping in InAs Quantum Dot Lasers on Silicon. *Appl Phys Lett* (2018) 113. doi:10.1063/1.5040792
 82. Wei W-Q, Feng Q, Guo J-J, Guo M-C, Wang J-H, Wang Z-H, et al. InAs/GaAs Quantum Dot Narrow Ridge Lasers Epitaxially Grown on SOI Substrates for Silicon Photonic Integration. *Opt Express* (2020) 28(18):26555–63. doi:10.1364/OE.402174
 83. Inoue D, Jung D, Norman J, Wan Y, Nishiyama N, Arai S, et al. Directly Modulated 13 μm Quantum Dot Lasers Epitaxially Grown on Silicon. *Opt Express* (2018) 26(6):7022–33. doi:10.1364/OE.26.007022
 84. Wan Y, Xiang C, Guo J, Koscica R, Kennedy M, Selvidge J, et al. High Speed Evanescent Quantum-Dot Lasers on Si. *Laser Photon Rev* (2021) 15(8):2100057. doi:10.1002/lpor.202100057
 85. Wan Y, Shang C, Norman J, Shi B, Li Q, Collins N, et al. Low Threshold Quantum Dot Lasers Directly Grown on Unpatterned Quasi-Nominal (001) Si. *IEEE J Select Top Quan Electron*. (2020) 26:1–9. doi:10.1109/jstqe.2020.2964381

86. Shi B, Pinna S, Zhao H, Zhu S, Klamkin J. Lasing Characteristics and Reliability of 1550 Nm Laser Diodes Monolithically Grown on Silicon. *Phys Status Solidi A* (2021) 218(3):2000374. doi:10.1002/pssa.202000374
87. Luo W, Xue Y, Huang J, Lin L, Shi B, Lau KM. Comparison of Growth Structures for Continuous-Wave Electrically Pumped 155 μm Quantum Dash Lasers Grown on (001) Si. *Photon Res* (2020) 8(12):1888–94. doi:10.1364/PRJ.403938
88. Zhu S, Shi B, Li Q, Lau KM. 1.5 μm Quantum-Dot Diode Lasers Directly Grown on CMOS-Standard (001) Silicon. *Appl Phys Lett* (2018) 113(22):221103. doi:10.1063/1.5055803
89. Liu AY, Peters J, Huang X, Jung D, Norman J, Lee ML, et al. Electrically Pumped Continuous-Wave 13 μm Quantum-Dot Lasers Epitaxially Grown on on-axis (001) GaP/Si. *Opt Lett* (2017) 42(2):338–41. doi:10.1364/OL.42.000338
90. Norman J, Kennedy MJ, Selvidge J, Li Q, Wan Y, Liu AY, et al. Electrically Pumped Continuous Wave Quantum Dot Lasers Epitaxially Grown on Patterned, on-axis (001) Si. *Opt Express* (2017) 25(4):3927–34. doi:10.1364/OE.25.003927
91. Jung D, Norman J, Kennedy MJ, Shang C, Shin B, Wan Y, et al. High Efficiency Low Threshold Current 1.3 μm InAs Quantum Dot Lasers on on-axis (001) GaP/Si. *Appl Phys Lett* (2017) 111(12):122107. doi:10.1063/1.4993226
92. Kwoen J, Jang B, Lee J, Kageyama T, Watanabe K, Arakawa Y. All MBE Grown InAs/GaAs Quantum Dot Lasers on on-axis Si (001). *Opt Express* (2018) 26(9):11568–76. doi:10.1364/OE.26.011568
93. D Jung, R Herrick, J Norman, Y Wan, AC Gossard, JE Bowers, editors. *High Performance and Reliable 1.3 μm InAs Quantum Dot Lasers Epitaxially Grown on Si. 2018 23rd Opto-Electronics And Communications Conference (OECC)*, 2018 (2018). p. 2–6.
94. B Villeneuve, M Cyr, HB Kim, editors. *High-stability Wavelength-Controlled DFB Laser Sources for Dense WDM Applications OFC '98 Opt Fiber Commun Conf Exhibit Tech Dig Conf Edition 1998 OSA Tech Dig Ser Vol2 (IEEE Cat No98CH36177)*, 1998 (1998). p. 22–7.
95. Coldren LA. Monolithic Tunable Diode Lasers. *IEEE J Select Top Quan Electron.* (2000) 6(6):988–99. doi:10.1109/2944.902147
96. Saruwatari M. All-optical Signal Processing for Terabit/second Optical Transmission. *IEEE J Select Top Quan Electron.* (2000) 6(6):1363–74. doi:10.1109/2944.902190
97. Tian B, Wang Z, Pantouvaki M, Absil P, Van Campenhout J, Merckling C, et al. Room Temperature O-Band DFB Laser Array Directly Grown on (001) Silicon. *Nano Lett* (2017) 17(1):559–64. doi:10.1021/acs.nanolett.6b04690
98. Wang Y, Chen S, Yu Y, Zhou L, Liu L, Yang C, et al. Monolithic Quantum-Dot Distributed Feedback Laser Array on Silicon. *Optica* (2018) 5(5):528–33. doi:10.1364/optica.5.000528
99. Wan Y, Norman JC, Tong Y, Kennedy MJ, He W, Selvidge J, et al. 1.3 Mm Quantum Dot-Distributed Feedback Lasers Directly Grown on (001) Si. *Laser Photon Rev* (2020) 14(7):2000037. doi:10.1002/lpor.202000037
100. Thompson MG, Rae AR, Mo Xia M, Pentry RV, White IH. InGaAs Quantum-Dot Mode-Locked Laser Diodes. *IEEE J Select Top Quan Electron.* (2009) 15(3):661–72. doi:10.1109/jstqe.2008.2012265
101. Liu S, Wu X, Jung D, Norman JC, Kennedy MJ, Tsang HK, et al. High-channel-count 20 GHz Passively Mode-Locked Quantum Dot Laser Directly Grown on Si with 41 Tbit/s Transmission Capacity. *Optica* (2019) 6(2):128–34. doi:10.1364/optica.6.000128
102. Dong B, de Labriolle XC, Liu S, Dumont M, Huang H, Duan J, et al. 1.3- μm Passively Mode-Locked Quantum Dot Lasers Epitaxially Grown on Silicon: Gain Properties and Optical Feedback Stabilization. *J Phys Photon* (2020) 2:045006. doi:10.1088/2515-7647/aba5a6
103. Wada K, Liu JF, Jongthammanurak S, Cannon DD, Danielson DT, Ahn DH, et al. Si Microphotonics for Optical Interconnection. In: L Pavesi G Guillot, editors. *Optical Interconnects: The Silicon Approach*. Berlin, Heidelberg: Springer (2006). p. 291–310.
104. Zhu S, Shi B, Wan Y, Hu EL, Lau KM. 155 μm Band Low-Threshold, Continuous-Wave Lasing from InAs/InAlGaAs Quantum Dot Microdisks. *Opt Lett* (2017) 42(4):679–82. doi:10.1364/OL.42.000679
105. Shi B, Klamkin J. Defect Engineering for High Quality InP Epitaxially Grown on on-axis (001) Si. *J Appl Phys* (2020) 127:033102. doi:10.1063/1.5127030
106. Li Q, Ng KW, Lau KM. Growing Antiphase-domain-free GaAs Thin Films Out of Highly Ordered Planar Nanowire Arrays on Exact (001) Silicon. *Appl Phys Lett* (2015) 106:072105. doi:10.1063/1.4913432
107. Shi B, Han Y, Li Q, Lau KM. 1.55- μm Lasers Epitaxially Grown on Silicon. *IEEE J Select Top Quan Electron.* (2019) 25(6):1–11. doi:10.1109/jstqe.2019.2927579
108. Zhu S, Shi B, Lau KM. Electrically Pumped 15 μm InP-Based Quantum Dot Microring Lasers Directly Grown on (001) Si. *Opt Lett* (2019) 44(18):4566–9. doi:10.1364/OL.44.004566
109. Wan Y, Jung D, Norman J, Shang C, MacFarlane I, Li Q, et al. O-band Electrically Injected Quantum Dot Micro-ring Lasers on on-axis (001) GaP/Si and V-Groove Si. *Opt Express* (2017) 25(22):26853–60. doi:10.1364/OE.25.026853
110. Wan Y, Norman J, Li Q, Kennedy MJ, Liang D, Zhang C, et al. 13 μm Submilliamp Threshold Quantum Dot Micro-lasers on Si. *Optica* (2017) 4(8):940–4. doi:10.1364/OPTICA.4.000940
111. Park J-S, Tang M, Chen S, Liu H. Monolithic III-V Quantum Dot Lasers on Silicon. In: DA Ritchie, editor. *Chapter Eleven - Monolithic III-V Quantum Dot Lasers on Silicon. Frontiers of Nanoscience*. Elsevier (2021). p. 353–88. doi:10.1016/b978-0-12-822083-2.00009-5
112. Wu J, Tang M, Liu H. Chapter 2-III-V Quantum Dot Lasers Epitaxially Grown on Si Substrates. In: C Tong C Jagadish, editors. *Nanoscale Semiconductor Lasers*. Elsevier (2019). p. 17–39. doi:10.1016/b978-0-12-814162-5.00002-9
113. Park J-S, Tang M, Chen S, Liu H. Heteroepitaxial Growth of III-V Semiconductors on Silicon. *Crystals* (2020) 10(12):1163. doi:10.3390/cryst10121163
114. Ying Z, Wang Z, Zhao Z, Dhar S, Pan DZ, Soref R, et al. Comparison of Microrings and Microdisks for High-Speed Optical Modulation in Silicon Photonics. *Appl Phys Lett* (2018) 112(11):111108. doi:10.1063/1.5019590
115. Zhou T, Tang M, Xiang G, Fang X, Liu X, Xiang B, et al. Ultra-low Threshold InAs/GaAs Quantum Dot Microdisk Lasers on Planar on-axis Si (001) Substrates. *Optica* (2019) 6(4):430–5. doi:10.1364/OPTICA.6.000430
116. Alcotte R, Martin M, Moeyaert J, Cipro R, David S, Bassani F, et al. Epitaxial Growth of Antiphase Boundary Free GaAs Layer on 300 Mm Si(001) Substrate by Metalorganic Chemical Vapour Deposition with High Mobility. *APL Mater* (2016) 4:046101. doi:10.1063/1.4945586
117. Tang M, Chen S, Wu J, Jiang Q, Kennedy K, Jurczak P, et al. Optimizations of Defect Filter Layers for 1.3- μm InAs/GaAs Quantum-Dot Lasers Monolithically Grown on Si Substrates. *IEEE J Select Top Quan Electron.* (2016) 22(6):50–6. doi:10.1109/jstqe.2016.2551941
118. George I, Becagli F, Liu HY, Wu J, Tang M, Beanland R. Dislocation Filters in GaAs on Si. *Semicond Sci Technol* (2015) 30(11):114004. doi:10.1088/0268-1242/30/11/114004
119. Liu HY, Sellers IR, Badcock TJ, Mowbray DJ, Skolnick MS, Groom KM, et al. Improved Performance of 1.3 μm Multilayer InAs Quantum-Dot Lasers Using a High-Growth-Temperature GaAs Spacer Layer. *Appl Phys Lett* (2004) 85(5):704–6. doi:10.1063/1.1776631
120. Zhou T, Tang M, Xiang G, Xiang B, Hark S, Martin M, et al. Continuous-wave Quantum Dot Photonic Crystal Lasers Grown on on-axis Si (001). *Nat Commun* (2020) 11(1):977. doi:10.1038/s41467-020-14736-9
121. Kobayashi W, Ito T, Yamanaka T, Fujisawa T, Shibata Y, Kurosaki T, et al. 50-Gb/s Direct Modulation of a 1.3- μm InGaAlAs-Based DFB Laser with a Ridge Waveguide Structure. *IEEE J Selected Top Quan Elect* (2013) 19(4):1500908. doi:10.1109/jstqe.2013.2238509
122. Chen R-Y, Chen Y-J, Chen C-L, Wei C-C, Lin W, Chiu Y-J. High-Power Long-Waveguide 1300-nm Directly Modulated DFB Laser for 45-Gb/s NRZ and 50-Gb/s PAM4. *IEEE Photon Technol Lett* (2018) 30(24):2091–4. doi:10.1109/LPT.1109/lpt.2018.2877676
123. Liang D, Huang X, Kurczveil G, Fiorentino M, Beausoleil RG. Integrated Finely Tunable Microring Laser on Silicon. *Nat Photon* (2016) 10:719–22. doi:10.1038/nphoton.2016.163
124. Kryzhanovskaya NV, Moiseev EI, Polubavkina YS, Maximov MV, Mokhov DV, Morozov IA, et al. Elevated Temperature Lasing from Injection Microdisk Lasers on Silicon. *Laser Phys Lett* (2018) 15:015802. doi:10.1088/1612-202x/aa9306
125. Ellis B, Mayer MA, Shambat G, Sarmiento T, Harris J, Haller EE, et al. Ultralow-threshold Electrically Pumped Quantum-Dot Photonic-crystal

- Nanocavity Laser. *Nat Photon* (2011) 5(5):297–300. doi:10.1038/nphoton.2011.51
126. Crosnier G, Sanchez D, Bouchoule S, Monnier P, Beaudoin G, Sagnes I, et al. Hybrid Indium Phosphide-On-Silicon Nanolaser Diode. *Nat Photon* (2017) 11(5):297–300. doi:10.1038/nphoton.2017.56
127. Lee YHD, Lipson M. Back-End Deposited Silicon Photonics for Monolithic Integration on CMOS. *IEEE J Selected Top Quan Elect* (2013) 19(2):8200207. doi:10.1109/jstqe.2012.2209865

Conflict of Interest: The authors declare that the research was conducted in the absence of any commercial or financial relationships that could be construed as a potential conflict of interest.

Publisher's Note: All claims expressed in this article are solely those of the authors and do not necessarily represent those of their affiliated organizations, or those of the publisher, the editors and the reviewers. Any product that may be evaluated in this article, or claim that may be made by its manufacturer, is not guaranteed or endorsed by the publisher.

Copyright © 2022 Cao, Park, Tang, Zhou, Seeds, Chen and Liu. This is an open-access article distributed under the terms of the Creative Commons Attribution License (CC BY). The use, distribution or reproduction in other forums is permitted, provided the original author(s) and the copyright owner(s) are credited and that the original publication in this journal is cited, in accordance with accepted academic practice. No use, distribution or reproduction is permitted which does not comply with these terms.